



MEDDOCS

Open Access Publisher

IMPORTANCE & APPLICATIONS OF NANOTECHNOLOGY

Deformation Defects on the Surface of Electrodeposited Nanocrystalline Metals

Oleg B Girin^{1*}; Ivan M Kuzyayev²

¹Department of Materials Science, Ukrainian State University of Chemical Technology, Gagarin Ave., 8, Dnipro 49005, Ukraine.

²Department of Innovative Engineering, Ukrainian State University of Chemical Technology, Gagarin Ave., 8, Dnipro 49005, Ukraine.

Corresponding Author: Oleg B Girin

Department of Materials Science, Ukrainian State University of Chemical Technology, Gagarin Ave., 8, Dnipro 49005, Ukraine.

Email: girin@ua.fm

Abstract

The state-of-the-art of the ideas about the phase formation in the electrodeposited metals used in medicine as coatings for instruments and various devices are considered. The developing concept of the phase formation in electrodeposited metals and alloys, based on the discovered phenomenon of the electrochemical phase formation in metals and alloys via a supercooled liquid state stage is discussed. The purpose of this study was to further experimental investigation of the phenomenon in point based on verification, analysis and modeling of the observed effect of plastic deformation of surface metal layers during their electrodeposition. Nickel having a nanocrystalline structure was chosen as a model electrodeposited metal; in the process of electrochemical phase formation, its surface was mechanically acted upon by moving nickel particles. The surface morphology of the resulting deposits was studied by scanning electron microscopy using the secondary electron imaging mode. The study has confirmed experimentally the appearance of deformation defects on the surface of metals in the course of their electrodeposition under external force acting at an angle to the crystallization front. It has been shown that a weak contact action exerted by particles of a metal on the surface of the same solid metal, cannot lead to plastic deformation of its surface layers. It has been concluded that deformation defects shaped as bands, furrows and plateaus arise due to the motion of solid metal particles over the still unsolidified surface of the metal that is in the process of electrodeposition. Mathematical models have been developed to model the motion of solid metal particles both in their oblique entry into the liquid surface of the electrodepositing metals and during their motion over the liquid surface of the electrodepositing metals, with the motion start in the horizontal plane. The findings serve as further evidence for the existence of the phenomenon of electrochemical phase formation in metals and alloys via a supercooled liquid state stage.

Published Online: Feb 12, 2021

eBook: Importance & Applications of Nanotechnology

Publisher: MedDocs Publishers LLC

Online edition: <http://meddocsonline.org/>

Copyright: © Girin OB (2021).

This chapter is distributed under the terms of Creative Commons Attribution 4.0 International License

Keywords: Deformation defect; Electrodeposited nanocrystalline metal; Modeling; Surface morphology.

Introduction

Deposits of electrodeposited metals are widely used in medicine as coatings for instruments, various devices, products and equipment for medical purposes. Nickel, chromium, silver, gold, copper and tin deposits obtained on medical devices by the method of electrodeposition (i.e. electroplating) substantially

increase their corrosion resistance, wear resistance, strength, and also improve their electrical and thermal conductivity characteristics. Application of nanotechnology to create a nanocrystalline structure in deposits of electrodeposited metals provides a significant improvement in their properties.

Citation: Girin OB, Kuzyayev IM, (2021). Deformation Defects on the Surface of Electrodeposited Nanocrystalline Metals. Importance & Applications of Nanotechnology, MedDocs Publishers. Vol. 6, Chapter 3, pp. 16-23.



Purposeful control of the properties of electrodeposited metals is possible based on the insight into their phase formation. Relatively recently, we have proposed a new concept of the phase formation in electrodeposited metals and alloys, based on the discovered phenomenon of the electrochemical phase formation in metals and alloys via a supercooled liquid state stage [1]. According to the concept proposed, the electrochemical deposition of a metal or alloy onto a solid cathode in an aqueous medium occurs via the formation of a supercooled metallic liquid as a multitude of liquid clusters of atoms, depositing in an avalanche-like manner in various places near the cathode or growing deposit, and its superfast solidification at the deposition temperature.

It should be noted that the proposed concept is fundamentally different from the existing concepts of the phase formation in electrodeposited metals and alloys [2-6]. According to these concepts, theoretically developed in recent publications [7-25], the phase formation in the material that is in the process of electrodeposition occurs by direct "incorporation" of ions from an aqueous solution or atoms, formed on its surface, into its crystal lattice. The existing concepts are far from answering the question of how the material ion, which is in the liquid phase with the amorphous structure of one substance (aqueous solution), is directly "incorporated" into the crystal lattice of the solid phase of another substance (material in the course of electrodeposition), and what phase transformations and structural changes occur during the process.

In recent years, a number of papers have been published (the most significant of them [26-32] are indexed by the Scopus database), in which the validity of the proposed concept is experimentally proved. Over the past two years (2019-2020) seven such papers (indexed by the Scopus database) have been published [33-39] in favor of the proposed concept.

One of the results in favor of the proposed concept is the revealed plastic deformation of surface layers of metals, which are in the process of electrodeposition, by solid particles moving under the action of a weak external force [32]. It was experimentally established that a weak force applied at an angle to the crystallization front to a metal in the process of its electrodeposition, leads to the appearance of plastic deformation bands on its surface. Such deformation bands result from the motion of already solidified particles over the surface of the still solidifying metal, when the particles simultaneously experience the force acting both parallel and perpendicular to the crystallization front.

It was of interest to elucidate the morphological features of the detected deformation defects and to model the motion of solid particles over the surface of a metal solidifying in the course of electrochemical deposition. Therefore, the purpose of this study was to further experimental investigation of the phenomenon in point based on verification, analysis and modeling of the observed effect of plastic deformation of surface metal layers during their electrodeposition.

Experimental

Nickel having a nanocrystalline structure was chosen as a model electrodeposited metal; in the process of electrochemical phase formation, its surface was mechanically acted upon by moving nickel particles. The choice of this metal was due to high values of hardness (up to 800 VHN [40]), featured by electrodeposited nickel.

Nickel deposits were obtained from a sulfate electrolyte at a temperature of 25 °C and a current density of 1.0 A/dm². The nickel current yield was 99.5 %, which is why the effect of hydrogen on the surface morphology of nickel deposits could be neglected. The surface morphology of the resulting deposits was studied by scanning electron microscopy (REM-1061) using the secondary electron imaging mode.

A weak external force was applied to nickel deposits in the course of electrodeposition, using a centrifugal plant and electrochemical cells described in [31]. To apply the external force at an angle to the deposit crystallization front, the cathode was placed in the electrochemical cell at an angle to its axis. Therefore, the external force did not act on the electrodeposited metal strictly perpendicular to the crystallization front, but at a certain angle to it. Centrifugal force proportional to overloads of 872g and 1256g was applied, which corresponds to the rotor angular speed of 2500 and 3000 min⁻¹.

Results

Deformation bands should be considered the main type of deformation defects detected on the surface of the investigated nickel deposits (Figure 1). These bands appeared when nickel particles moved under the action of centrifugal force over the deposit surface being formed. A specific feature of these defects was the fact that the bands passed through the body of grain aggregates, but not along their boundaries, which indicated a deformation of the deposit surface layers, characteristic of a non-solid state.

If we assume that the deposit was in a solid state during the deformation, then the bands should be expected to have uneven edges outlined by grain boundaries. However, Figure 1a shows that the bands have smooth, sharply defined edges, similar to the edges of defects arising in the process of deformation of a viscous non-solid material. Moreover, as seen from Figure 1b, the inner edges of the band exhibit a non-crystalline nature of deformation, which is characteristic of the non-solid state.

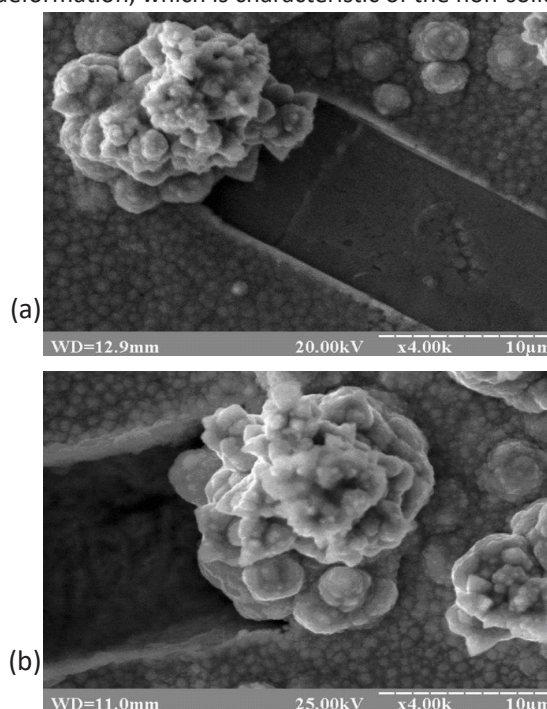


Figure 1: SEM images of band deformation defects on the surface of nickel deposits, electrodeposited under the action of external force proportional to an overload of 872g at an angle to the crystallization front.

It should be noted that in the case of such deformation of the solid deposit, the so-called "deformation accordion" of the surface layers should form on its surface, which is characteristic of the final section of the band. However, Figure 1 indicates the absence of such formations behind the particle in the direction of its movement.

Figure 2 shows that with an increase in the overload, a characteristic relief formed by protruding sections of the particle appears on the horizontal area of the band (Figure 2a). The occurrence of areas of solidified foam at the edges of the band should be considered another feature of the deformation bands that appeared under an increased overload due to the deformation effect on the solidifying metal (Figure 2b).

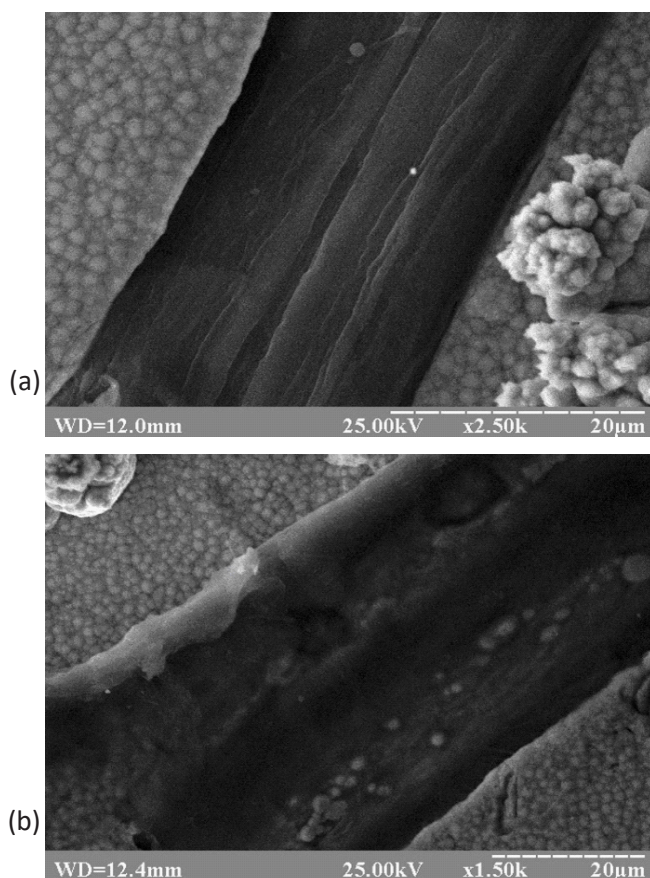


Figure 2: SEM images of the deformation defects shaped as bands on the surface of nickel deposits, electrodeposited under the action of external force proportional to an overload of 1256g at an angle to the crystallization front.

Furrows (Figure 3a) and plateaus (Figure 3b) should be considered other types of deformation defects that appeared on the surface of nickel deposits in the course of electrodeposition under an external force at an angle to the crystallization front. A defect shaped as a narrow elongated furrow appeared apparently due to the contact action by the protrusion of a moving particle on the surface layer of nickel that was in the process of electrodeposition. Figure 3a clearly shows the smoothed side surface of the furrow, which can be explained in two ways: Either it was formed by a material significantly exceeding nickel in hardness, or nickel, while electrodepositing, was in a non-solid state at the moment of its deformation by the nickel particle.

A large-area plateau formed on the surface of the nickel deposit by a whole ensemble of moving nickel particles suggests that the plastic deformation of the deposit occurred during the period of electrodeposition when the surface layer was in a non-crystalline state. Otherwise, we would have to admit that

the hardness of the moving particles of the electrodeposited nickel was significantly higher than the hardness of the electrodeposited nickel deposit. If we reject this statement as absurd, then we should admit that a still solidifying, but not solidified deposit was exposed to the deformation by nickel particles in the process of electrochemical deposition of nickel.

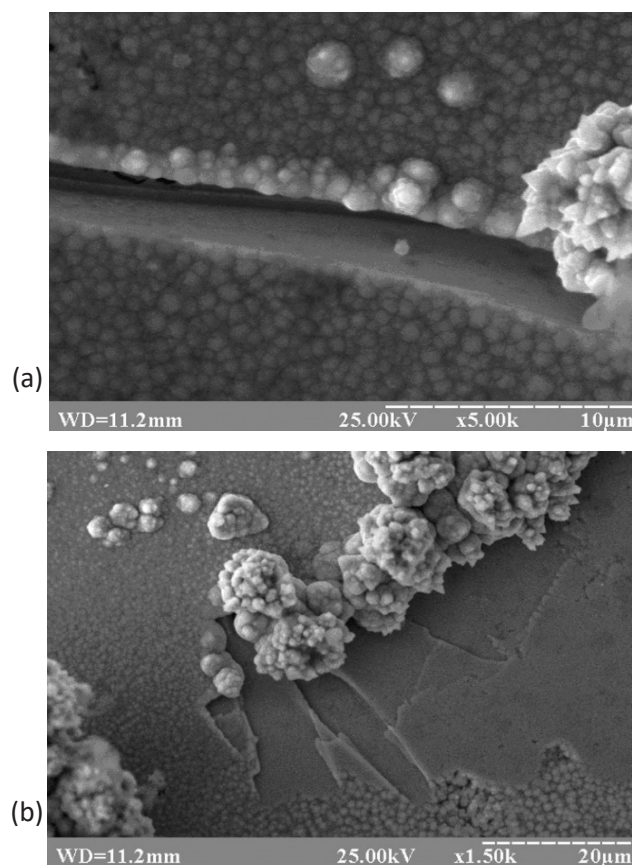


Figure 3: SEM images of deformation defects shaped as a furrow (a) or a plateau (b) on the surface of nickel deposits, electrodeposited under the action of external force proportional to an overload of 872g at an angle to the crystallization front.

As follows from the data presented, a weak contact action upon the surface of a solid material by particles of the same material could not lead to plastic deformation of its surface layers. Consequently, the obtained experimental results indicate that, in the process of electrochemical phase formation, metals and alloys pass an intermediate stage of liquid state.

Discussion

Hardness is known to be the property of the surface layer of a metal to resist plastic deformation induced by contact action from another, harder body [41]. Therefore, in the absence of the intermediate stage of the liquid state in nickel while it is electrodepositing, nickel particles moving over the surface of the forming nickel deposit could not leave any traces of plastic deformation on its growing surface.

This is explained by the fact that the hardness of nickel surface in the course of electrodeposition and of nickel particles in contact with it is absolutely the same. Moreover, the hardness of the nickel deposit is high enough to expect that deformation bands or furrows on its surface could be left by any by-products of electrochemical nickel deposition, which contact its surface.

On the other hand, stress required for the onset of plastic deformation of a material is estimated as the yield strength [41]. According to [42], the yield strength of nickel is 83 MPa.

Therefore, a compressive stress of not lower than 83 MPa should be expected in the surface layers of electrodepositing nickel to induce plastic deformation of solid nickel deposits by moving particles.

However, as shown in [31], even at the maximum value of the overload coefficient in the performed experiments ($k = 1256$), the stress created by the centrifugal force in the electrodepositing nickel deposits does not exceed 0.748 MPa. This stress is less than one percent of the above-mentioned yield strength of nickel, which is far from sufficient to induce plastic deformation of solid nickel deposits. Consequently, the occurrence of the detected deformation defects on the surface of the investigated nickel deposits cannot be explained by plastic deformation of the nickel layers in the solid state.

In this regard, the detected plastic deformation of the surface of the growing nickel deposit by nickel particles can be logically explained by the presence of an intermediate stage of the liquid state in nickel while it is electrodepositing. If this is the case, then previously solidified nickel particles could well leave deformation bands on the solidifying surface of the deposit while moving over it during electrodeposition under an external force directed at an angle to the crystallization front (Figure 1 and 2).

Again, if a cluster of solid particles moves over the surface of the still solidifying deposit, the surface layers may be smoothed out and form a plateau (Figure 3b). In addition, the furrows could be well left by solid nickel particles detached from the solidifying surface of the deposit when they come in contact with the still unsolidified surface during electrodeposition under external force acting at an angle to the crystallization front (Figure 3a).

Modeling

Mathematical modeling was performed using differential equations of motion, which describes the law of conservation of momentum, and the equation of continuity, which describes the law of conservation of mass [43-45].

The equation of motion in vector form (regardless of the selected coordinate system) has the following form

$$\rho \cdot \frac{D\vec{V}}{Dt} = -\nabla P + \left[\nabla \times \overset{\leftrightarrow}{\sigma} \right] \pm \rho \cdot \vec{g} + \vec{F}_i \quad (1)$$

where ρ is the density of the material; t is time; \vec{v} is velocity vector of material motion; $D\vec{v}/Dt$ is substantial derivative of the \vec{v} vector; ∇P is the pressure gradient; $\overset{\leftrightarrow}{\sigma}$ is the stress tensor; $[\nabla \times \overset{\leftrightarrow}{\sigma}]$ is a vector product of ∇ vector by $\overset{\leftrightarrow}{\sigma}$ tensor; \vec{g} is the free fall acceleration vector; \vec{F}_i is additional forces caused by different energy fields per unit volume; ∇ is a vector that has the form

$$\nabla = \delta_1 \frac{\partial}{\partial x_1} + \delta_2 \frac{\partial}{\partial x_2} + \delta_3 \frac{\partial}{\partial x_3} \quad (2)$$

where δ_i are unit vectors; x_i are coordinate axes (x, y, z).

The left-hand side of equation (1) is the inertial term of the equation of motion, that is, it is the product of acceleration and mass per unit volume. The right-hand side includes the following terms: The first (after the equal sign) is a force exerted by pressure per unit volume; the second term is forces exerted by

intermolecular transfer, also per unit volume; the third term is forces of gravity per unit volume (mass forces); the fourth term is the centrifugal force per unit volume.

The equation of continuity in vector form for an incompressible fluid can be represented as follows

$$\left(\nabla \cdot \vec{V} \right) = 0 \quad (3)$$

To solve the differential equations in the obtained mathematical models, we used the corresponding software product from the MathCAD package.

Given that the deformation defects found on the surface of electrodeposits could arise under the centrifugal force both as a result of an oblique entry of detached solid particles into the solidifying surface of the deposit with their subsequent motion, and as a result of the ordinary motion of particles over the deposit surface, we used two corresponding modeling options.

Modeling the motion of a solid metal particle in its oblique entry into the liquid surface of the electrodepositing metal

For brevity, we take the following terms: A solid metal particle - solid; the liquid surface of a metal that is in the process of electrodeposition - liquid medium. Then, according to the oblique entry pattern presented in Figure 4, the solid moves from position 1_a at an angle β to the horizontal axis x . Entering the liquid medium 2 and contacting the metal substrate (or previously solidified layers) 3, the solid starts moving from position 1_b in the direction x . The LHS of the problem is to find the path traversed by solid 1 in liquid medium 2 (Figure 4).

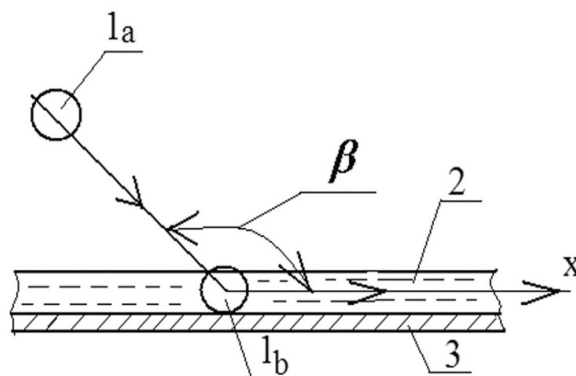


Figure 4: Calculated schematic of oblique impact.

To construct a mathematical model, we will take into account only the x -component of the velocity in the equations of motion, and its change only along the coordinate x . We will neglect forces exerted by mass.

Then the equation of motion (1) for the Cartesian coordinate system in projections onto the axis x will have the form

$$\rho_l \cdot \left(\frac{\partial V_x}{\partial t} + V_x \cdot \frac{\partial V_x}{\partial x} \right) = -\frac{\partial P}{\partial x} + \frac{\partial \sigma_{xx}}{\partial x} + F_c \quad (4)$$

where ρ_l is the density of the liquid medium; F_c is the centrifugal force, which can be determined from the expression

$$F_c = \rho \cdot \omega^2 \cdot x \quad (5)$$

where ω is the rotation frequency of the system under consideration.

The solution of equation (4) will be sought taking into account the dependence for the velocity on the left-hand side of this equation in the form $V_x = \partial x / \partial t$.

The stress component σ_x for a non-Newtonian (power-law) fluid in the case of non-shear (longitudinal) motion can be represented as

$$\sigma_{xx} = 2 \cdot \mu_0 \cdot \left| \frac{\partial V_x}{\partial x} \right|^{n-1} \cdot \frac{\partial V_x}{\partial x}, \quad (6)$$

where μ_0 is flow consistency coefficient; n is the power law index.

We express the pressure P through the force of the medium resistance to the penetration of solids $P = -F$, which in a general form can be determined from the expression

$$F = F_1 + F_2, \quad (7)$$

where F_1 is the force of dynamic resistance; F_2 is the force exerted by the viscosity of the medium.

The first component of the force is induced by the inertia of the medium particles and its value can be taken proportional to the square of the penetration rate. As for the second component, it arises due to overcoming the friction between the medium particles and can be taken proportional to the penetration rate.

The components F_1 and F_2 are represented as follows

$$\left. \begin{aligned} F_1 &= -\rho_s \cdot V_x^2, \\ F_2 &= -\mu_0 \cdot \left| \frac{\partial V_x}{\partial x} \right|^{n-1} \cdot V_x \cdot k_g. \end{aligned} \right\} \quad (8)$$

where ρ_s is the density of the solid; k_g is the geometric parameter of a solid, which is determined from the expression

$$k_g = \frac{S_{mid}}{V_g}, \quad (9)$$

where S_{mid} , V_g are the midsection area and volume of the solid, respectively.

Taking into account expressions (6) and (8), equation (4) in the stationary approximation can be written as follows (given the equal densities of the liquid medium in the process of solidification and of the solid body, which have the same nature $\rho_l = \rho_s = \rho$)

$$\frac{d^2 V_x}{dx^2} = \frac{-\mu_0 \cdot k_g \cdot \left| \frac{dV_x}{dx} \right|^n - \rho \cdot \omega^2 \cdot x}{\mu_0 \cdot \left| \frac{dV_x}{dx} \right|^{n-2} \cdot \left(k_g \cdot (n-1) \cdot V_x^{2 \cdot n} \cdot \left| \frac{dV_x}{dx} \right| \right)} \quad (10)$$

The solution of equation (10) using the mathematical package MathCAD under specified system parameters is shown in Figure 5.

It is easy to check that for the selected system parameters in a sufficiently wide range of their values, Eq. (10) can be replaced by a simpler equation, namely

$$\frac{d^2 V_x}{dx^2} = \frac{1}{(1-n) \cdot V_x} \cdot \left| \frac{dV_x}{dx} \right|^2. \quad (11)$$

The solution of equation (11) is shown in Figure 6. In this case, the following parameters of the motion were taken: $\beta = 100 \text{deg}$; $V_x(0) = 0,016 \text{m/s}$; $dV_x(0)/dx = -5,671 \text{s}^{-1}$; $R = 40 \cdot 10^{-6} \text{m}$; $\rho = 8,8 \cdot 10^3 \cdot \text{kg/m}^3$; $\mu_0 = 10^3 \cdot \text{Pa} \cdot \text{m}^n$; $n = 0,16$; $\omega = 10 \cdot \text{s}^{-1}$.

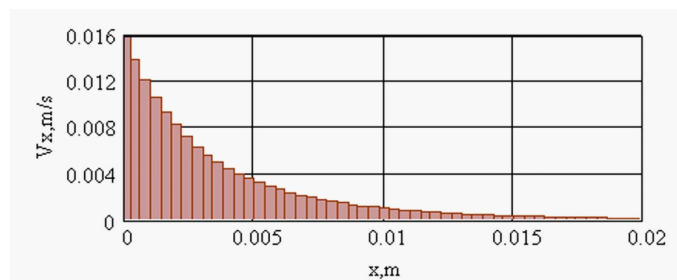


Figure 5: Flat graph of velocity V_x distribution according to equation (10).

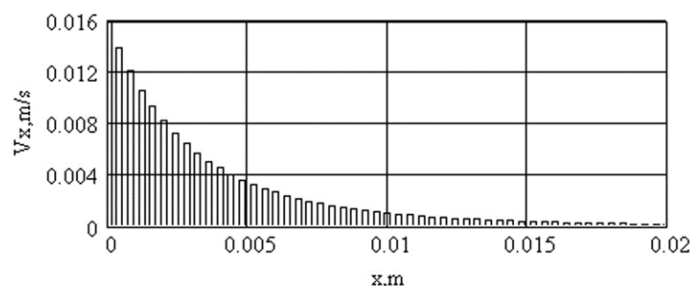


Figure 6: Flat graph of velocity V_x distribution according to equation (11).

Equation (11), up to notations, coincides with the equation given in [46]

$$y \cdot \frac{d^2 y}{dx^2} = a \cdot \left| \frac{dy}{dx} \right|^2. \quad (12)$$

The last two equations use the following relationships in the notation: $y = V_x$; $a = 1/(1-n)$. Then the solution to Eq. (11) at $a \neq 1$ will have the form

$$V_x = |C_1 \cdot x + C_0|^{n1}, \quad (13)$$

where $n1 = (n-1)/n$.

The solution by formula (13) is shown in Figure 7.

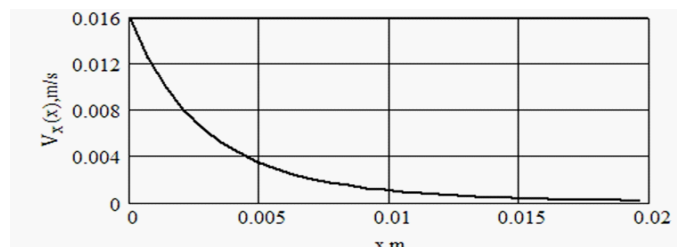


Figure 7: Flat graph of velocity V_x distribution according to equation (13).

As can be seen from Figures 5-7, all the three models, namely (10), (11) and (13), give the same results. Consequently, the simpler formula (13) is advisable to be used for the mathematical description of the motion of solid metal particles in their oblique entry into the liquid surface of electrodepositing metals.

Modeling the motion of a solid metal particle over the liquid surface of the electrodepositing metal, with the motion start in the horizontal plane

The above mathematical models describe the motion of a solid metal particle in its oblique entry into the liquid phase of the electrodepositing metal and its further motion over the surface of the deposit. However, the formation of the described deformation defects is possible not only in the oblique entry of a particle into the liquid phase, but also during the usual rectilinear motion of an already solidified particle along the still unsolidified surface of the deposit under an external force of various nature, for example, the centrifugal force.

In this case, due to the extremely uneven formation and growth of the deposit on the cathode surface, which is a well-known fact [47], some particles, having passed into the solid state and being exposed to a force exceeding their adhesion to the still unsolidified deposit and directed at an angle to the crystallization front, start moving on the surface of the deposit. The motion of the particles begins in the horizontal plane with zero initial values of velocity and velocity gradients along the corresponding coordinate axes.

The equation of forces equilibrium, which in this case is equivalent to the equation of motion, can be presented as follows

$$F_{mc} + F_{fr} = F_c, \quad (14)$$

where F_{mc} the forces of molecular transfer in the liquid are phase; F_{fr} are the forces of frontal resistance when a solid moves in a liquid phase; F_c are centrifugal forces.

All the forces in equation (14) are taken per unit volume. The forces given on the left hand side of equation (14) can be determined by the following expressions

$$F_{mc} = \eta(x) \cdot \frac{d^2V_x}{dx^2}; \quad (15)$$

$$F_{fr} = \eta(x) \cdot \left(k_g \cdot \frac{dV_x}{dx} + k_g^2 \cdot V_x \right). \quad (16)$$

In the last two expressions, the value k_g is found from equation (9), and the parameter $\eta(x)$ is the viscosity coefficient, which in the general case depends on time, but in this case we will express the dependence of the viscosity coefficient on the x coordinate. Then the functional dependence for the viscosity coefficient can be expressed by the following equation

$$\eta(x) = 2 \cdot \eta_0 \cdot \exp\left(-\frac{x}{\beta}\right), \quad (17)$$

where η_0 the initial is value of the viscosity coefficient; β is the growth rate of the viscosity coefficient.

For centrifugal force, expression (5) will be true.

Substituting the corresponding expressions into equation (14) and getting rid of the coefficients for the highest derivative of the velocity V_x , we obtain the following second-order differential equation

$$\frac{d^2V_x}{dx^2} + a \cdot \frac{dV_x}{dx} + b \cdot V_x = d \cdot x \cdot \exp\left(-\frac{x}{\beta}\right), \quad (18)$$

where $a = k_g$, $b = k_g^2$, $d = \frac{\rho \cdot \omega^2}{2 \cdot \eta_0}$.

The solution of equation (18) is shown in Figure 8 and found using the mathematical package MathCAD with the following parameters: $\omega = 10^2 \text{ s}^{-1}$; $\rho = 8620 \cdot \text{kg/m}^3$;

$R_{mid} = 40 \cdot 10^{-6} \text{ m}$ $\eta_0 = 10 \cdot \text{Pa} \cdot \text{s}$; $\beta = 3 \cdot 10^{-3} \text{ m}$;
Solution results were obtained using the rkfixed function.

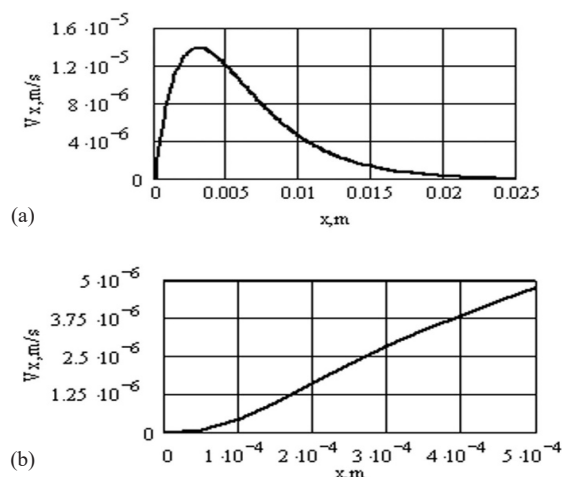


Figure 8: Graphs of velocity distribution with the motion starting in the horizontal plane; the graphs were obtained in the interval: $x = 0..0.025 \text{ m}$ (a); $x = 0..5 \cdot 10^{-4} \text{ m}$ (b).

It should be noted that equation (18) is the equation of forced oscillations [46]. The solution to this equation can be obtained in an analytical form. Here, in the general case, three versions of the homogeneous equation are valid: (a) $\lambda^2 = a^2 - 4 \cdot b > 0$; (b) $\lambda^2 = 4 \cdot b - a^2 > 0$; (c) $4 \cdot b = a^2$.

If we take the parameters graphically represented in Figure 8 as initial data, then option (b) will be valid, for which we have. $4 \cdot b - a^2 = 1.055 \cdot 10^9 \text{ m}^{-2}$ Then the solution of the homogeneous equation can be written as

$$V_x = \exp(-a \cdot x/2) \cdot \left[C_1 \cdot \cos\left(\frac{\lambda \cdot x}{2}\right) + C_2 \cdot \sin\left(\frac{\lambda \cdot x}{2}\right) \right], \quad (19)$$

The homogeneous equation (19) should be supplemented with the solution of the inhomogeneous equation in the form

$$V_x = 2 \cdot d/\lambda \cdot \int_0^x \psi \cdot \exp\left(-\frac{\psi}{\beta}\right) \cdot \exp\left[\frac{a \cdot (\psi - x)}{2}\right] \cdot \sin\left[\frac{\lambda \cdot (x - \psi)}{2}\right] d\psi, \quad (20)$$

Finally, after determining the constants of integration, taking into account zero initial conditions, and after the corresponding transformations, we obtain the following equation for the functional dependence of the velocity on the coordinate X and the growth rate of the viscosity coefficient β

$$V_x(x, \beta) = \frac{2 \cdot K(\beta)}{\lambda} \cdot \left[f1(x, \beta) \cdot \exp\left(-\frac{x}{\beta}\right) + 4 \cdot \beta^2 \cdot \exp\left(-\frac{x \cdot k_g}{2}\right) \cdot f2(x, \beta) \right], \quad (21)$$

$$\text{where ; } K(\beta) = \frac{d}{(4 - 4 \cdot k_g \cdot \beta + k_g^2 \cdot \beta^2 + \lambda^2 \cdot \beta^2)^2},$$

$$f1(x, \beta) = 2 \cdot \lambda \cdot \beta^2 \cdot (4 \cdot x - 4 \cdot x \cdot k_g \cdot \beta + x \cdot k_g^2 \cdot \beta^2 + x \cdot \lambda^2 \cdot \beta^2 + 8 \cdot \beta - 4 \cdot k_g \cdot \beta^2);$$

$$f2(x, \beta) = -4 \cdot \lambda \cdot \beta \cdot \cos(\lambda \cdot x/2) + 2 \cdot \lambda \cdot \beta^2 \cdot k_g \cdot \cos(\lambda \cdot x/2) + 4 \cdot \sin(\lambda \cdot x/2) - 4 \cdot k_g \cdot \beta \cdot \sin(\lambda \cdot x/2) + k_g^2 \cdot \beta^2 \cdot \sin(\lambda \cdot x/2) - \lambda^2 \cdot \beta^2 \cdot \sin(\lambda \cdot x/2)$$

The solution results are shown in Figure 9; the graphs presented were obtained with the following general parameters: $\omega = 1000 \cdot 1/s$; $\rho = 1000 \cdot \text{kg}/\text{m}^3$; $R_{\text{mid}} = 40 \cdot \text{m}$; $\eta_0 = 10 \cdot \text{Pa} \cdot \text{s}$.

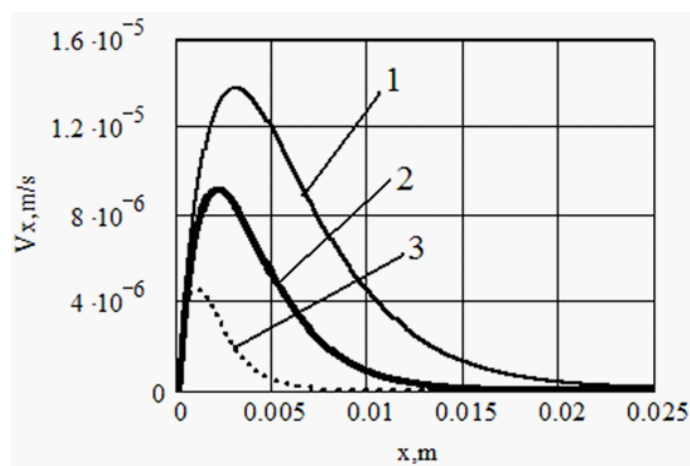


Figure 9: Graphs of the velocity distribution with the motion start in the horizontal plane; the graphs were obtained by the formula (21) at varied values of the growth rate of the viscosity coefficient: 1 – $\beta = 0,003\text{m}$; 2 – $\beta = 0,002\text{m}$; 3 – $\beta = 0,001\text{m}$.

Comparison of the graphs in Figure 8a and Figure 9 (curve 1) showed their complete coincidence. Therefore, formula (21) can be used for calculations that model the motion of solid metal particles over the liquid surface of electrodepositing metals with the motion start in the horizontal plane.

Conclusions

The study has confirmed experimentally the appearance of deformation defects on the surface of metals in the course of their electrodeposition under external force acting at an angle to the crystallization front. It has been shown that a weak contact action exerted by particles of a metal on the surface of the same solid metal, cannot lead to plastic deformation of its surface layers. It has been concluded that deformation defects shaped as bands, furrows and plateaus arise due to the motion of solid metal particles over the still unsolidified surface of the metal that is in the process of electrodeposition. Mathematical models have been developed to model the motion of solid metal particles both in their oblique entry into the liquid surface of the electrodepositing metals and during their motion over the liquid surface of the electrodepositing metals, with the motion start in the horizontal plane. The obtained experimental results in combination with the performed modeling indicate that in the

process of electrochemical phase formation, metals and alloys pass an intermediate stage of the liquid state.

References

- Girin OB, Khlyntsev VP. Mechanism of liquid phase formation in metals during electrodeposition. *Elektronnaya Obrabotka Materialov (Soviet Surface Engineering and Applied Electrochemistry)*. 2000; 3: 13-18.
- Milchev A. *Electrocrystallization. Fundamentals of Nucleation and Growth*. New York: Kluwer. 2002.
- Paunovic M, Schlesinger M. *Fundamentals of Electrochemical Deposition*. Hoboken: Wiley. 2006.
- Budevski E, Staikov G, Lorenz WJ. *Electrochemical Phase Formation and Growth*. Weinheim: Wiley. 2008.
- Plieth W. *Electrochemistry for Materials Science*. Amsterdam: Elsevier. 2008.
- Gamburg YuD, Zangari G. *Theory and Practice of Metal Electrodeposition*, New York: Springer-Verlag. 2011.
- Budevski EB, Staikov GT, Lorenz WJ. Electrocrystallization nucleation and growth phenomena. *Electrochimica Acta*. 2000; 45: 2559-2574.
- Hyde ME, Compton RG. A review of the analysis of multiple nucleation with diffusion controlled growth. *Journal of Electroanalytical Chemistry*. 2003; 549: 1-12.
- Bicelli LP, Bozzini B, Mele C, D'Urzo L. A review of nanostructural aspects of metal electrodeposition. *International Journal of Electrochemical Science*. 2008; 3: 356-408.
- Milchev A. Electrocrystallization: Nucleation and growth of nano-clusters on solid surfaces. *Russian Journal of Electrochemistry*. 2008; 44: 619-648.
- Torrent-Burgues J. Electrochemical nucleation: Comparison test of classical and atomistic nucleation models. *Journal of Solid State Electrochemistry*. 2013; 17: 373-378.
- Isaev VA, Grishenkova OV. Galvanostatic phase formation. *Journal of Solid State Electrochemistry*. 2014; 18: 2383-2386.
- Milchev A. *Nucleation phenomena in electrochemical systems: Kinetic models*. ChemTexts. 2016; 2: 1-9.
- Chen J, Luo S, Liu Y, Chen S. Theoretical analysis of electrochemical formation and phase transition of oxygenated adsorbates on Pt (111). *ACS Applied Materials and Interfaces*. 2016; 8: 20448-20458.
- Milchev A. Electrochemical phase formation: Classical and atomistic theoretical models. *Nanoscale*. 2016; 8: 13867-13872.
- Altimari P, Pagnanelli F. Electrochemical nucleation and three-dimensional growth under mixed kinetic-diffusion control: Analytical approximation of the current transient. *Electrochimica Acta*. 2016; 205: 113-117.
- Altimari P, Pagnanelli F. Electrochemical nucleation and three-dimensional growth of metal nanoparticles under mixed kinetic-diffusion control: Model development and validation. *Electrochimica Acta*. 2016; 206: 116-126.
- Romero-Romo M, Aldana-Gonzalez J, Botello LE, Montes de Oca MG, Ramirez-Silva MT, et al. Electrochemical nucleation and growth of Cu onto Au nanoparticles supported on a Si (111) wafer electrode. *Journal of Electroanalytical Chemistry*. 2017; 791: 1-7.
- Mladenova E, Milchev A. Electrochemical nucleation and growth

- of three-dimensional clusters: The case of multi-step ions discharge. *Journal of Solid State Electrochemistry*. 2017; 21: 1599-1604.
20. Sebastian P, Botello LE, Valles E, Gomez E, Palomar-Pardave M, et al. Three-dimensional nucleation with diffusion controlled growth: A comparative study of electrochemical phase formation from aqueous and deep eutectic solvents. *Journal of Electroanalytical Chemistry*. 2017; 793: 119-125.
 21. Nath P, Pandey R, Das A, Mallik A. Effect of deposition potential and copper concentration on the phase transformation mechanism and structural distribution during electrodeposition of Ni-Cu magnetic alloy thin films. *Metallic Materials*, 2017; 55: 255-265.
 22. Brankovic SR. Fundamentals of metal deposition via surface limited redox replacement of underpotentially-deposited monolayer. *Electrochemical Society Interface*. 2018; 27: 57-63.
 23. Zhou X, Wang Y, Liang Z, Jin H. Electrochemical deposition and nucleation/growth mechanism of Ni-Co-Y₂O₃ multiple coatings. *Materials*. 2018; 11: 1124-1132.
 24. Isaev VA, Grishenkova OV, Zaykov YP. Theory of cyclic voltammetry for electrochemical nucleation and growth. *Journal of Solid State Electrochemistry*. 2018; 22: 2775-2778.
 25. Sides WD, Huang Q. Electrochemical nucleation and growth of antimony telluride binary compound on gold substrate. *Journal of the Electrochemical Society*. 2018; 165: D568-D573.
 26. Girin OB. Phase transformations in the metallic materials being electrodeposited and their application for the development of advanced technologies for anticorrosive protection of canned-food steel sheet. *Materials Science Forum*. 2007; 561-565: 2369-2372.
 27. Girin OB. Phase and structure formation of metallic materials electrodeposited via a liquid state stage: New experimental proof. *Defect and Diffusion Forum*. 2010; 303-304: 99-105.
 28. Girin OB, Ovcharenko VI. Formation of spherulites and pentagonal quasicrystals in metals being electrodeposited. *Eastern-European Journal of Enterprise Technologies*. 2014; 2/11: 30-34.
 29. Girin OB, Kuzyayev IM. Dynamic behavior of gas nano-sized bubbles in liquid phase of the metal being electrodeposited. *Journal of Nano- and Electronic Physics*. 2016; 8: 01034.
 30. Girin OB. Further evidence of phase formation through a liquid state stage in metals being electrodeposited: Part 1. *Surface Engineering and Applied Electrochemistry*. 2017; 53: 137-143.
 31. Girin O.B. Further evidence of phase formation through a liquid state stage in metals being electrodeposited: Part 2. *Surface Engineering and Applied Electrochemistry*. 2017; 53: 233-239.
 32. Girin OB. Further evidence of phase formation through a liquid state stage in metals being electrodeposited: Part 3. *Surface Engineering and Applied Electrochemistry*. 2017; 53: 339-344.
 33. Girin OB. Electrochemical amorphous phase formation in metals. *Journal of Chemical Technology and Metallurgy*. 2019; 54: 391-396.
 34. Girin OB, Korolyanchuk DG. Electrochemical reduction of ions in metals/alloys at a liquid cathode versus a solid chemically identical one. *Scientific Study & Research: Chemistry & Chemical Engineering, Biotechnology, Food Industry*. 2019; 20: 639-642.
 35. Girin OB, Ovcharenko VI, Korolyanchuk DG. Features of texture formation in polymorphic metals being electrodeposited. *Acta Metallurgica Slovaca*. 2019; 25: 267-275.
 36. Girin O., Kuzyayev I., Nikolsky V., Yaris V. Discovering and modelling the wave-like shapes on the surface of metal deposits, being electrodeposited under the force impact. *Key Engineering Materials*. 2020; 844: 135-145.
 37. Girin OB, Korolyanchuk DG. Electrochemical phase formation of metals and alloys at chemically identical solid or liquid cathode: Part 1. Metals. *Surface Engineering and Applied Electrochemistry*. 2020; 56: 28-40.
 38. Girin OB, Korolyanchuk DG. Electrochemical phase formation of metals and alloys at chemically identical solid or liquid cathode: Part 2. Alloys in the form of substitutional solid solutions. *Surface Engineering and Applied Electrochemistry*. 2020; 56: 289-300.
 39. Girin OB, Korolyanchuk DG. Electrochemical phase formation of metals and alloys at chemically identical solid or liquid cathode: Part 3. Alloys in the form of intermetallic compounds. *Surface Engineering and Applied Electrochemistry*. 2020; 56: 501-509.
 40. Tuck J, Korsunsky AM, Davidson R, Bull SJ, Elliott DM. Modelling of the hardness of electroplated nickel coatings on copper substrates. *Surface and Coatings Technology*. 2000; 127: 1-8.
 41. McLean D. *Mechanical Properties of Metals*. New York: R.E. Krieger Pub. Co. 1977.
 42. Baucchio M. *ASM Metals Reference Book*. Materials Park: ASM International. 1997.
 43. Bird RB, Armstrong RS, Hassager O. *Dynamics of Polymeric Liquids*. Vol. 1. Fluid Mechanics. New York: Wiley. 1977.
 44. Bohme G. *Stromungsmechanik Nicht-Newtonscher Fluids*. Stuttgart: B.G. Teubner. 1981.
 45. Jing Z, Daming W, Kuzyayev I.M, Weihong C, Hong X, et al. Study of solid-plug conveying in a centrifugal extruder. *International Polymer Processing*. 2008; 23: 286-291.
 46. Камке Э. *Справочник по обыкновенным дифференциальным уравнениям*. Москва: Наука. 1971.
 47. McVay L, Muller RH, Tobias CW. Application of videomicroscopy to in-situ studies of electrodeposition. *Journal of the Electrochemical Society*. 1989; 136: 3384-3387.